AIP | Applied Physics Letters

Vapor transport deposition and epitaxy of orthorhombic SnS on glass and NaCl substrates

Artit Wangperawong, Steven M. Herron, Rory R. Runser, Carl Hägglund, Jukka T. Tanskanen et al.

Citation: Appl. Phys. Lett. **103**, 052105 (2013); doi: 10.1063/1.4816746
View online: http://dx.doi.org/10.1063/1.4816746
View Table of Contents: http://apl.aip.org/resource/1/APPLAB/v103/i5
Published by the AIP Publishing LLC.

Vapor transport deposition and epitaxy of orthorhombic SnS on glass and NaCl substrates

Artit Wangperawong,[1] Steven M. Herron,[1] Rory R. Runser,[2] Carl Hägglund,[1] Jukka T. Tanskanen,[1] Han-Bo-Ram Lee,[3] Bruce M. Clemens,[1] and Stacey F. Bent[1,a)]
[1]*Stanford University, Stanford, California 94305, USA*
[2]*University of California at Berkeley, Berkeley, California 94720, USA*
[3]*Incheon National University, Yeonsu-gu, Incheon, South Korea*

(Received 23 May 2013; accepted 9 July 2013; published online 30 July 2013)

Polycrystalline SnS, Sn_2S_3, and SnS_2 were deposited onto glass substrates by vapor transport deposition, with the stoichiometry controlled by deposition temperature. In addition, epitaxial growth of orthorhombic SnS(010) films on NaCl(100) with thicknesses up to 600 nm was demonstrated. The in-plane [100] directions of SnS and NaCl are oriented approximately 45° apart, and the translational relationship between SnS and NaCl was predicted by density functional theory. The epitaxial SnS is p-type with carrier concentration on the order of 10^{17} cm^{-3} and Hall hole mobility of 385 cm^2 V^{-1} s^{-1} in-plane. It has indirect and direct bandgaps of 1.0 and 2.3 eV, respectively. © *2013 AIP Publishing LLC*. [http://dx.doi.org/10.1063/1.4816746]

SnS is a natively p-type semiconductor known to have favorable optical properties for solar cells, e.g., a suitable bandgap (1.1–1.3 eV) and high absorption coefficient.[1] In addition to photovoltaics, properly oriented SnS is advantageous for thermoelectric applications.[2] Because its constituents are non-toxic and earth abundant, efficient devices made of SnS would be highly attractive. However, although the Shockley-Queisser limit for SnS is around 24%, the highest solar power conversion efficiency of SnS devices reported to date is 2.04% using polycrystalline SnS.[3] Since open-circuit voltage was a major shortcoming for the record device, proper band alignment at layer interfaces, surface passivation, and higher minority carrier lifetime and mobility within SnS solar cells could improve their performance.

This study demonstrates growth using vapor transport deposition (VTD) of the thermodynamically stable phase of SnS, which is a layered compound with orthorhombic structure wherein the chalcogen layers are bound by interlayer van der Waals interactions.[4] Since reconstruction and dangling bonds are ideally not present on surfaces cleaved along these layers,[5] properly architected SnS devices may be alleviated of surface recombination and Fermi level pinning. We demonstrate in this study that the top and bottom surfaces of SnS thin films can be terminated by these layers via epitaxial growth. Epitaxial growth may also allow for higher quality material as well as *in-situ* doping control. For these reasons, epitaxially grown SnS could offer more pathways toward higher efficiency SnS devices. Epitaxial growth of orthorhombic SnS has been reported by molecular beam epitaxy (MBE) onto graphene[6] and MgO,[7] by vacuum evaporation onto NaCl,[8,9] and by electrodeposition onto Au in the form of nanodisks.[10] Here, we present a VTD process to epitaxially grow orthorhombic SnS thin films on NaCl as well as characterize the optoelectronic properties of the resulting films.

Our VTD process differs from conventional vacuum evaporation processes in that the trajectory of the vapor to the deposition surface is not in the line-of-sight of the evaporation source. Predicated on the ability of SnS to sublimate congruently and condense stoichiometrically,[11] VTD of SnS is potentially compatible with commercial manufacturing such as that used for CdTe solar cells.[12,13] SnS's relatively high vapor pressure and an enthalpy of sublimation[11] very similar to that of CdTe (Ref. 14) facilitates VTD at reasonable source temperatures (<800 °C) under moderate vacuum (<100 Torr). Our VTD procedure consists of heating 99.5% tin (II) sulfide powder (Alfa Aesar) in a multizone horizontal tube furnace to 425 °C with the substrate 4 in. downstream of the source and maintained at 365 °C. The base pressure of the system is 5 mTorr, several orders of magnitude higher than in MBE and other vacuum evaporation systems. The deposition time was varied to achieve the desired thickness. For instance, 24 h of deposition yielded 600 nm thick SnS films on NaCl(100).

As a control study, we first performed VTD of SnS onto glass substrates. The anisotropic growth of the layered compound resulted in blade-like morphology when deposited in polycrystalline form (Fig. 1(a)). In addition to SnS, polycrystalline Sn_2S_3 and SnS_2 were deposited in the same process further downstream at substrate temperatures in the ranges of 335 to 350 °C and 320 to 335 °C, respectively (Figs. 1(b) and 1(c)). The observed deposits were grey, black, and yellow, respectively. The tin sulfide morphologies for each phase are all similarly bladed, and the corresponding symmetric (θ–2θ) X-ray diffraction (XRD) patterns obtained with a PANalytical X'Pert PRO diffractometer (Cu radiation, 45 kV, 40 mA) identify each of them (Figs. 1(d)–1(f)). Condensation occurs in the order of SnS, Sn_2S_3, and SnS_2 most likely because of the respective vapor pressures over condensed phases, which is lowest for SnS and highest for SnS_2.[11] The deposition of both Sn_2S_3 and SnS_2 diminished with successive heating of the powder source. XRD patterns (not shown) of untreated SnS powder and VTD-processed SnS powder suggest that Sn_2S_3 and SnS_2 exist as impurities in the original SnS powder source and are vaporized by

a)Author to whom correspondence should be addressed. Electronic mail: sbent@stanford.edu.

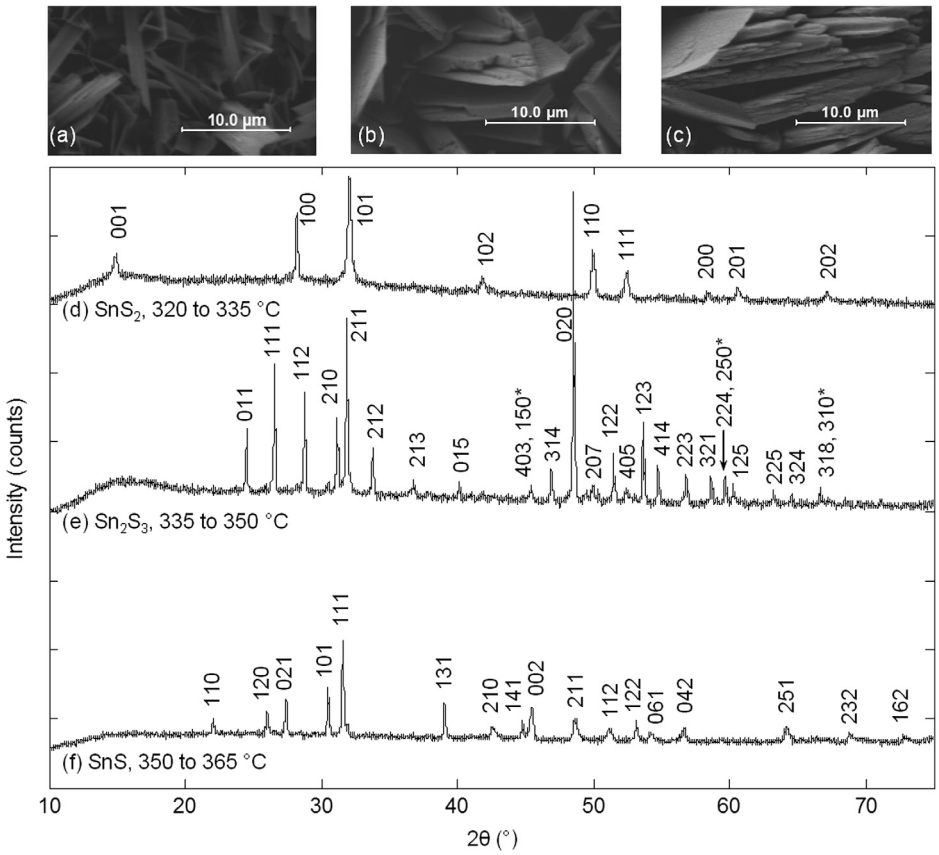

FIG. 1. Plan view SEM images and corresponding indexed $\theta-2\theta$ XRD patterns[30] for polycrystalline tin sulfide deposited by VTD onto glass substrates at temperatures of 365 °C and below. The presence of SnS_2 (a, d), Sn_2S_3 (b, e), and SnS (c, f) phases depends on substrate temperature. Possible SnS peaks in (e) are indexed to planes denoted with *.

fractional distillation, leading to depletion of these phases with repeated heating.

To demonstrate SnS heteroepitaxy onto NaCl(100), a freshly cleaved NaCl crystal was used as the substrate. The resulting films were specularly reflective. Examination of the film growth in its early stages reveals what appears to be initial nucleation (Fig. 2(a)) and coalescence (Fig. 2(b)). Indicative of epitaxial growth, the rectangular edges of the SnS nuclei and coalesced islands are largely aligned with the NaCl substrate (Fig. 2(b), inset). We speculate that the sequence of film growth involves first a uniform distribution of nuclei after vapor exposure onto the substrate (Fig. 2(a)). It next appears that coalescence decreases the island density (Fig. 2(b)). In the cross-sectional SEM image of a 600 nm thick SnS film on NaCl (Fig. 3), the sheet-like stacking morphology observed suggests preferential orientation such that the (010) planes are parallel to the nominal sample surface. As mentioned above, the bonding between (010) planes is through weak van der Waals interactions, so surface reconstruction and dangling bonds may be absent from the top and bottom surfaces of the deposited film.

Indeed while θ–2θ XRD patterns show that SnS, Sn_2S_3, and SnS_2 deposited onto glass substrates adopt various orientations (Fig. 1), those from SnS deposited onto NaCl(100) show that it is preferentially oriented with (010) planes parallel to the nominal sample surface (Fig. 4). In a θ–2θ XRD scan, the scattering vector is perpendicular to the sample surface and therefore diffraction only occurs from atomic planes parallel to the surface. To obtain the in-plane orientation, XRD pole figures were performed by fixing 2θ to probe either NaCl(111) or SnS(111) reflections while measuring the diffracted intensity as a function of the sample tilt (χ) and out-of-plane rotation (φ). The result shown in the inset of Fig. 4 reveals that the [100] directions of NaCl and the SnS are oriented approximately 45° with respect to one another. While the NaCl(111) peaks occur at χ of 55° and φ angles

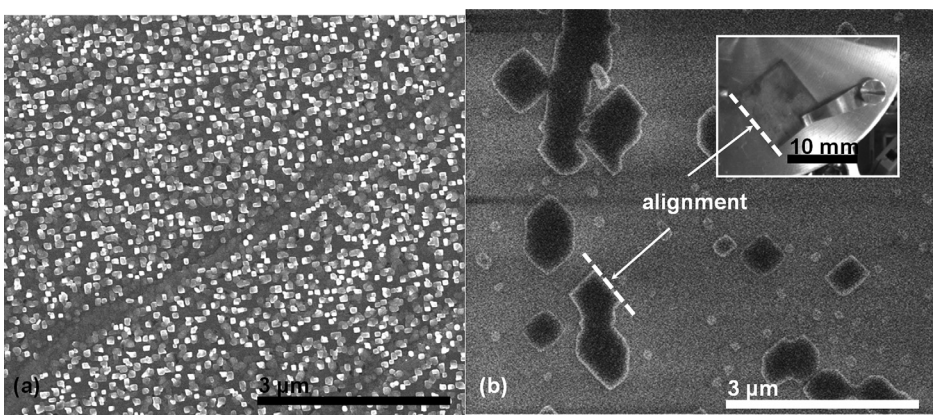

FIG. 2. Plan view SEM images of early stages of growth, exhibiting (a) small nuclei and (b) islands coalescing with (inset) photograph of sample taken inside the SEM chamber. In both images, the straight edges of the SnS are generally aligned with NaCl ⟨100⟩ (oriented differently between (a) and (b)). The dashed white lines are a guide to the eye to illustrate alignment.

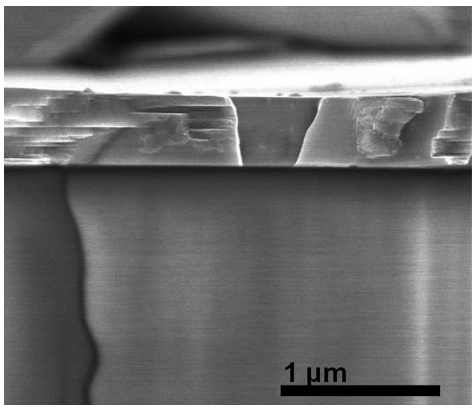

FIG. 3. Cross-sectional SEM of SnS(010) thin film grown epitaxially on NaCl(100). The film is approximately 600 nm thick.

90° apart, the SnS(111) peaks occur at χ of 75° and φ angles of 95° and 85° apart. These angles suggest that orthorhombic SnS with its 2-fold symmetric (010) plane predominantly adopts a single orientation when grown epitaxially on NaCl.

To determine the NaCl/SnS interface structure and its implications on the SnS(010) film position on NaCl(100), we performed a full structural relaxation of a NaCl/SnS interface model, which was composed of six NaCl(100) layers and two SnS layers oriented as suggested by XRD. The calculations were performed using the CRYSTAL09 (Ref. 15) program, a 4 × 4 slab unit cell, the PBE0 (Refs. 16 and 17) functional, def2-SVP[18–20] basis for Sn, S, and Cl, and a 8–511G (Ref. 21) basis for Na. The structural optimization suggests the relationship shown in the interface model of Fig. 5. The optimized system was verified as the true local minimum structure by vibrational analysis. The simulation results agree with XRD measurements in that [100] directions of NaCl and the SnS are oriented approximately 45° with respect to one another. Furthermore, the results suggest that the Sn and S atoms are not located directly above the Na and Cl ions at the interface. Rather, the atoms in the SnS layer right above NaCl are located between the surface cations and anions.

Although reports of SnS growth on alkali halides date back as far as 1962,[8,9,22–24] those results either included a mixture of orthorhombic and cubic phases or were not fully characterized to establish the epitaxial relationship between

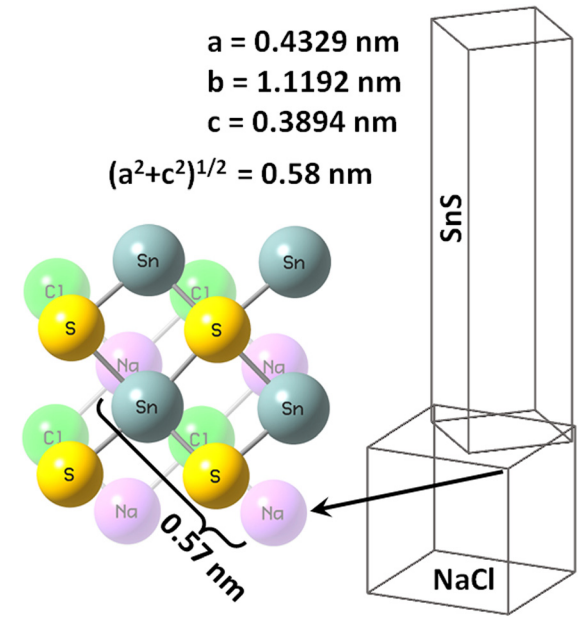

FIG. 5. Illustration of the epitaxial relationship between SnS and NaCl unit cells accompanying the interface structure predicted by periodic density functional theory (DFT) calculations. For clarity, in the top view of the PBE0-optimized NaCl/SnS interface (left), only the SnS layer closest to the NaCl surface is illustrated.

the deposited film and the substrate. Our XRD data above as well as TEM measurements on samples after dissolution of the NaCl substrate with water (see Fig. 6) both reveal only orthorhombic SnS features. This study not only demonstrates epitaxial growth of orthorhombic SnS on NaCl but also suggests an interface structure between the two materials. Such information could benefit studies of SnS heteroepitaxy on other substrates, which would be useful for multijunction and heterojunction solar cell applications. Furthermore, knowledge of the crystal orientation allows us to exploit anisotropic properties of the material.

Hall measurements using the Van der Pauw method show that the epitaxial SnS is p-type with carrier concentration on the order of $10^{17}\,\mathrm{cm}^{-3}$ and hole mobility of $385\,\mathrm{cm}^2\,\mathrm{V}^{-1}\,\mathrm{s}^{-1}$ in-plane. Mobility measurements were not reported for the record SnS solar cell, for which the SnS was deposited (not epitaxially) by chemical vapor deposition.[3] However, the same

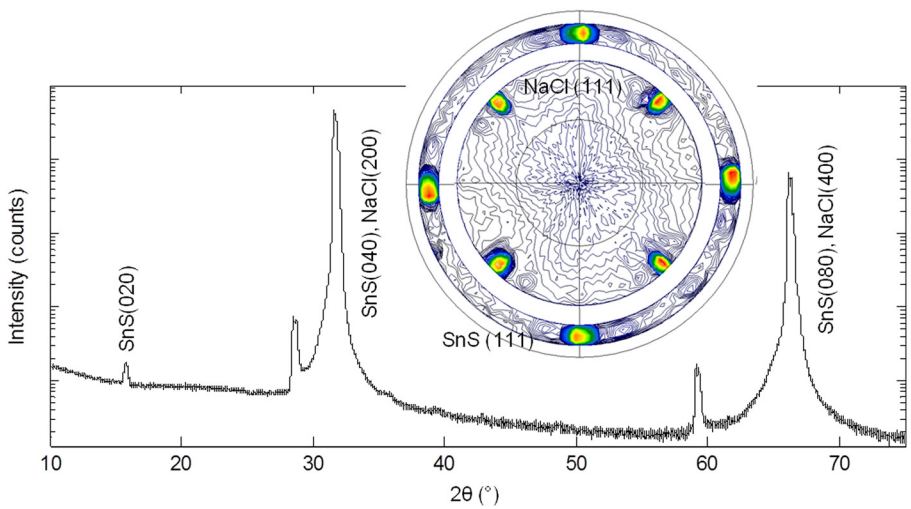

FIG. 4. θ–2θ XRD scan of SnS thin film grown on NaCl with combined XRD pole figure scans of NaCl(111) and SnS(111) shown in the inset. Unlabeled peaks are due to Cu $K\beta$ radiation.

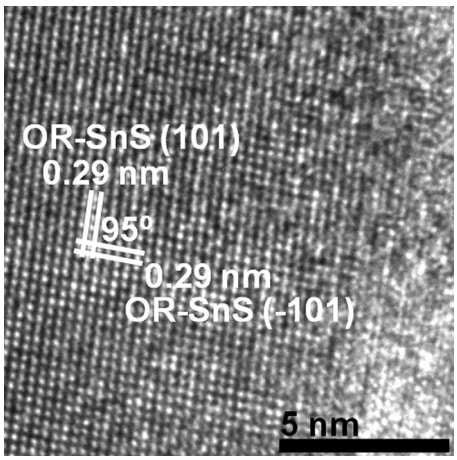

FIG. 6. TEM image of SnS after dissolution of NaCl substrate annotated with planar spacings and dihedral angle representative of the orthorhombic SnS (010) cleavage plane.

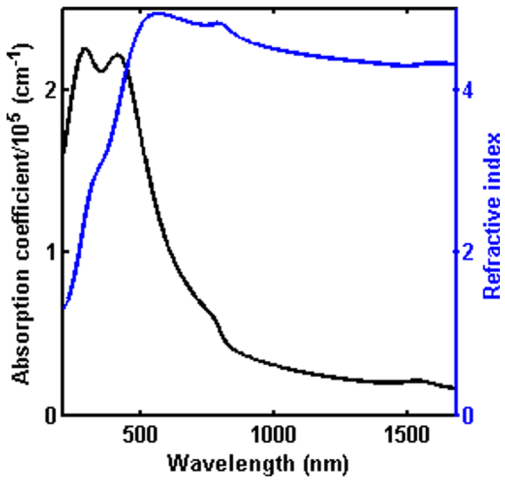

FIG. 7. Refractive index and absorption coefficient derived from ellipsometry measurements.

authors reported in a preceding publication that atomic layer deposited, non-epitaxial SnS had Hall ⟨010⟩ hole mobilities in the range of 0.82–13.8 $cm^2\ V^{-1}\ s^{-1}$.[26] As the typical Van der Pauw setup measures mobility only within the plane of the films, in order to compare, we estimate the ⟨010⟩ hole mobility of our epitaxial SnS film to be about 80 $cm^2\ V^{-1}\ s^{-1}$ based on SnS single crystal measurements showing that in-plane mobility is about 5 times greater than that out-of-plane.[25] Mobility is expected to be higher in epitaxial films due to decreased grain boundary scattering. Since electron mobility is affected by the same scattering mechanisms,[12] we also expect correlation between electron and hole mobility values within the same material. Higher electron mobility is desirable for higher efficiency p-type absorbers such as SnS because minority carrier transport contributes to photocurrent and voltage.

To determine the optical properties of the epitaxial films, spectroscopic ellipsometry using a Woollam M2000 instrument was performed on the SnS layers on NaCl over a spectral range from 210 to 1688 nm. The SnS layer was modeled as a uniform thickness layer with homogeneous optical constants represented by oscillator functions (a polynomial spline function near the absorption onset and three harmonic oscillators at higher energies). The layer thickness and oscillator parameters were fitted to minimize the root mean square error of the model output versus the measured ellipsometric data. The resulting refractive index and absorption coefficient are shown in Fig. 7. The bandgaps of the heteroepitaxially deposited orthorhombic SnS thin films are 1.0 eV indirect and 2.3 eV direct according to Tauc plot analyses.

The SnS layer can be isolated either by mechanical exfoliation or by dissolving away with water the underlying NaCl substrate. Energy-dispersive X-ray spectroscopy measurements (not shown) collected after dissolution of the substrate do not detect residual sodium or chlorine in the product. Although we have attempted to fabricate complete solar cell devices using the isolated SnS thin film, cracks in the film caused severe electrical shunts. We attribute these cracks, which formed between domains of SnS on the order of 100 μm in size, to the in-plane thermal expansion coefficient mismatch between NaCl and SnS over the temperature range of 20 to 365 °C. Moreover, upon heating SnS contracts in ⟨100⟩ and expands in ⟨001⟩. Based on published data for NaCl (Ref. 27) and SnS,[28] the maximum thermal strain in this temperature range is 2.8%. We believe that higher efficiency SnS devices are attainable if the cracks can be mitigated, and we are thus currently developing an approach to deposit SnS onto substrates maintained at lower temperatures.

In summary, we have developed a VTD approach that does not require ultra-high vacuum and can separately deposit SnS, Sn_2S_3, and SnS_2. Orthorhombic SnS(010) was epitaxially grown on NaCl(100) and an interface structure is proposed. Our epitaxial SnS films exhibit promising optical and electrical properties as a solar cell absorber layer, but its thermal expansion mismatch with the NaCl substrate induces cracks detrimental to solar cell performance. One solution we are testing is to deposit SnS onto substrates maintained at lower temperatures. In addition to being an absorber layer, SnS grown by VTD may also be useful as p-type back contacts in CdTe devices,[12] serving a role as the selective back contact similar to what has been reported about $MoSe_2$ in copper indium gallium (di)selenide solar cells.[29]

The authors are grateful to Professor Yi Cui for use of a multizone tube furnace to perform the VTD experiments and to Dr. Arturas Vailionis for helpful XRD-related discussions. This study is based upon the work supported by the Department of Energy (DOE) through the Bay Area Photovoltaic Consortium under Award No. DE-EE0004946. A.W. is supported by the DOE Office of Science Graduate Fellowship Program (DOE SCGF), made possible in part by the American Recovery and Reinvestment Act of 2009, administered by ORISE-ORAU under Contract No. DE-AC05-06OR23100. J.T.T. gratefully acknowledges the Academy of Finland (Grant 256800/2012) and the Finnish Cultural Foundation for financial support.

[1]K. T. R. Reddy, N. K. Reddy, and R. W. Miles, Sol. Energy Mater. Sol. Cells **90**, 3041 (2006).
[2]D. Parker and D. J. Singh, J. Appl. Phys. **108**, 083712 (2010).

[3]P. Sinsermsuksakul, K. Hartman, S. B. Kim, J. Heo, L. Sun, H. H. Park, R. Chakraborty, T. Buonassisi, and R. G. Gordon, Appl. Phys. Lett. **102**, 053901 (2013).
[4]L. A. Burton and A. Walsh, J. Phys. Chem. C **116**, 24262 (2012).
[5]*Photoelectrochemistry and Photovoltaics of Layered Semiconductors*, edited by A. Aruchamy (Kluwer Academic Publishers, Dordrecht, The Netherlands, 1992).
[6]W. Wang, K. K. Leung, W. K. Fong, S. F. Wang, Y. Y. Hui, S. P. Lau, Z. Chen, L. J. Shi, C. B. Cao, and C. Surya, J. Appl. Phys. **111**, 093520 (2012).
[7]H. Nozaki, M. Onoda, M. Sekita, K. Kosuda, and T. Wada, J. Solid State Chem. **178**, 245 (2005).
[8]S. B. Badachhape and A. Goswami, Indian J. Pure Appl. Phys. **2**, 250 (1964).
[9]B. F. Bilenkii, A. G. Mikolaichuk, and D. M. Freik, Phys. Status Solidi **28**, K5 (1968).
[10]S. Boonsalee, R. V. Gudavarthy, E. W. Bohannan, and J. A. Switzer, Chem. Mater. **20**, 5737 (2008).
[11]V. Piacente, S. Foglia, and P. Scardala, J. Alloys Compd. **177**, 17 (1991).
[12]*Handbook of Photovoltaic Science and Engineering*, edited by A. Luque and S. Hegedus (John Wiley and Sons, 2003).
[13]R. C. Powell, NREL Subcontract Report SR-520-39669, First Solar, 2006.
[14]G. Bardi, K. Leronimakis, and G. Trionfetti, Thermochim. Acta **129**, 341 (1988).
[15]R. Dovesi, V. R. Saunders, C. Roetti, R. Orlando, C. M. Zicovich-Wilson, F. Pascale, B. Civalleri, K. Doll, N. M. Harrison, I. J. Bush, Ph. D'Arco, and M. Llunell, CRYSTAL09 User's Manual, Torino, Italy, 2009.
[16]J. Perdew, K. Burke, and M. Ernzerhof, Phys. Rev. Lett. **77**, 3865 (1996).
[17]C. Adamo and V. Barone, J. Chem. Phys. **110**, 6158 (1999).
[18]A. J. Karttunen, T. F. Fassler, M. Linnolahti, and T. A. Pakkanen, Inorg. Chem. **50**, 1733 (2011).
[19]A. Schaefer, H. Horn, and R. Ahlrichs, J. Chem. Phys. **97**, 2571 (1992).
[20]F. Weigend and R. Ahlrichs, Phys. Chem. Chem. Phys. **7**, 3297 (2005).
[21]R. Dovesi, C. Roetti, C. Freyria-Fava, M. Prencipe, and V. R. Saunders, Chem. Phys. **156**, 11 (1991).
[22]S. B. Badachhape and A. Goswami, J. Phys. Soc. Jpn. **17**, 251 (1962).
[23]A. N. Mariano and K. L. Chopra, Appl. Phys. Lett. **10**, 282 (1967).
[24]A. G. Mikolaichuk and D. M. Freik, Sov. Phys. Solid State **11**, 2033 (1970).
[25]W. Albers, C. Haas, H. J. Vink, and J. D. Wasscher, J. Appl. Phys. **32**, 2220 (1961).
[26]P. Sinsermsuksakul, J. Heo, W. Noh, A. S. Hock, and R. G. Gordon, Adv. Energy Mater. **1**, 1116 (2011).
[27]F. D. Enck and J. G. Dommel, J. Appl. Phys. **36**, 839 (1965).
[28]H. Wiedemeier and F. J. Csillag, Z. Kristallogr. **149**, 17 (1979).
[29]K. L. Chopra, P. D. Paulson, and V. Dutta, Prog. Photovoltaics **12**, 69 (2004).
[30]Powder Diffraction File (PDF) database, International Centre for Diffraction Data, Card Nos. 01-075-0367, 04-007-0816, 04-004-3833.